View metadata, citation and similar papers at core.ac.uk

brought to you by CORE

provided by Harvard University - DASH

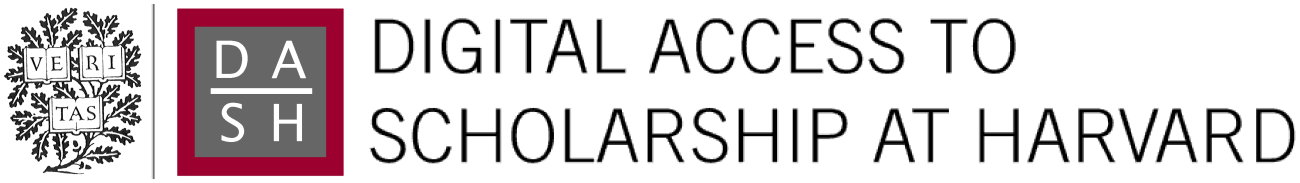


# Transition Metal-Catalyzed Oxidation of Atmospheric Sulfur: Global Implications for the Sulfur Budget

The Harvard community has made this article openly available. Please share how this access benefits you. Your story matters.

| | |
|---|---|
| **Citation** | Alexander, Becky, Rokjin J. Park, Daniel J. Jacob, and Sunling Gong. 2009. "Transition Metal-Catalyzed Oxidation of Atmospheric Sulfur: Global Implications for the Sulfur Budget." Journal of Geophysical Research: Atmospheres 114 (D2): D02309. doi:10.1029/2008jd010486. http://dx.doi.org/10.1029/2008JD010486. |
| **Published Version** | doi:10.1029/2008jd010486 |
| **Accessed** | April 17, 2018 4:45:56 PM EDT |
| **Citable Link** | http://nrs.harvard.edu/urn-3:HUL.InstRepos:11923057 |
| **Terms of Use** | This article was downloaded from Harvard University's DASH repository, and is made available under the terms and conditions applicable to Other Posted Material, as set forth at http://nrs.harvard.edu/urn-3:HUL.InstRepos:dash.current.terms-of-use#LAA |

*(Article begins on next page)*

# Transition metal-catalyzed oxidation of atmospheric sulfur: Global implications for the sulfur budget

Becky Alexander,[1] Rokjin J. Park,[2] Daniel J. Jacob,[3] and Sunling Gong[4]

Received 23 May 2008; revised 15 September 2008; accepted 4 November 2008; published 30 January 2009.

[1] We use observations of the oxygen-17 excess ($\Delta^{17}O$) of sulfate in the Arctic to quantify the sulfate source from aqueous $SO_2$ (S(IV)) oxidation by $O_2$ catalyzed by transition metals. Due to the lack of photochemically produced OH and $H_2O_2$ in high latitudes during winter, combined with high anthropogenic $SO_2$ emissions in the Northern Hemisphere, oxidation by $O_3$ is predicted to dominate sulfate formation during winter in this region. However, $\Delta^{17}O$ measurements of sulfate aerosol collected in Alert, Canada, are not consistent with $O_3$ as the dominant oxidant and indicate that a S(IV) oxidant with near-zero $\Delta^{17}O$ values ($O_2$) is important during winter. We use a global chemical transport model to interpret quantitatively the Alert observations and assess the global importance of sulfate production by Fe(III)- and Mn(II)-catalyzed oxidation of S(IV) by $O_2$. We scale anthropogenic and natural atmospheric metal concentrations to primary anthropogenic sulfate and dust concentrations, respectively. The solubility and oxidation state of these metals is determined by cloud liquid water content, source, and sunlight. By including metal-catalyzed S(IV) oxidation, the model is consistent with the $\Delta^{17}O$ magnitudes in the Alert data during winter. Globally, we find that this mechanism contributes 9–17% to sulfate production. The inclusion of metal-catalyzed oxidation does not resolve model discrepancies with surface $SO_2$ and sulfate observations in Europe. Oxygen isotope measurements of sulfate aerosols collected near anthropogenic and dust sources of metals would help to verify the importance of this sulfur oxidation pathway.

**Citation:** Alexander, B., R. J. Park, D. J. Jacob, and S. Gong (2009), Transition metal-catalyzed oxidation of atmospheric sulfur: Global implications for the sulfur budget, *J. Geophys. Res.*, *114*, D02309, doi:10.1029/2008JD010486.

## 1. Introduction

[2] Sulfate is a major component of the atmospheric aerosol and drives the formation of new aerosol particles through nucleation. The implications for scattering of solar radiation and for cloud microphysics represent one of the largest uncertainties in current assessments of climate change [*Solomon et al.*, 2007]. Sulfate is mainly produced within the atmosphere by oxidation of $SO_2$, which is itself directly emitted (fossil fuel combustion, industrial processes, volcanoes) or produced within the atmosphere by oxidation of reduced sulfur species such as dimethyl sulfide (DMS) emitted by oceanic phytoplankton. $SO_2$ is then lost from the atmosphere through dry deposition at the surface or oxidation to sulfate. The oxidation of $SO_2$ can take place in the gas phase [*Stockwell and Calvert*, 1983] and in the aqueous phase [*Schwartz*, 1987].

[3] The primary oxidants for atmospheric oxidation of $SO_2$ on the global scale are thought to be OH, $H_2O_2$ and $O_3$. Gas-phase oxidation of $SO_2$ by OH

$$\begin{aligned} &SO_2 + OH + M \rightarrow HOSO_2 + M \\ (R1)\quad &HOSO_2 + O_2 \rightarrow HO_2 + SO_3 \\ &SO_3 + H_2O + M \rightarrow H_2SO_4 + M \end{aligned}$$

produces $H_2SO_4$(g) that can nucleate new particles under favorable conditions, increasing aerosol number density and the population of cloud condensation nuclei (CCN) [*Andronache et al.*, 1997; *Kumala et al.*, 2000; *Weber et al.*, 2001]. Sulfate produced in the aqueous phase is present in larger particles and does not lead to nucleation of new particles. Aqueous-phase sulfate formation involves dissolution of $SO_2$ followed by acid-base dissociation of $SO_2 \cdot H_2O$ to $HSO_3^-$ ($pK_{a1} = 1.9$) and $SO_3^{2-}$ ($pK_{a2} = 7.2$). We refer to total dissolved $SO_2$ as S(IV) $\equiv SO_2 \cdot H_2O + HSO_3^- + SO_3^{2-}$. Oxidation of S(IV) takes place by dissolved $H_2O_2$

$$(R2a)\qquad HSO_3^- + H_2O_2 \leftrightarrow SO_2OOH^- + H_2O$$

$$(R2b)\qquad SO_2OOH^- + H^+ \rightarrow H_2SO_4$$

[1]Department of Atmospheric Sciences, University of Washington, Seattle, Washington, USA.
[2]School of Earth and Environmental Sciences, Seoul National University, Seoul, Korea.
[3]School of Engineering and Applied Sciences and Department of Earth and Planetary Sciences, Harvard University, Cambridge, Massachusetts, USA.
[4]Air Quality Research Division, Environment Canada, Toronto, Ontario, Canada.

Copyright 2009 by the American Geophysical Union.
0148-0227/09/2008JD010486

and dissolved $O_3$

$$(R3) \qquad O_3 + SO_3^{2-} \rightarrow O_2 + SO_4^{2-}$$

S(IV) can also be oxidized in the aqueous phase by other oxidants including $O_2$ catalyzed by Fe(III) and Mn(II) [*Hoffmann and Jacob*, 1984], $NO_2$ [*Lee and Schwartz*, 1983], $NO_3$ [*Feingold et al.*, 2002], and $HNO_4$ [*Dentener et al.*, 2002; *Warneck*, 1999]. These other oxidants are thought to be of little importance on a global scale, although they may be significant regionally. HOCl and HOBr have been proposed as potentially important S(IV) oxidants in the marine boundary layer [*Vogt et al.*, 1996; *von Glasow et al.*, 2002], but there is so far no observational evidence.

[4] A comparison of 11 large-scale atmospheric sulfate aerosol models (COSAM), found that models tend to predict surface level sulfate aerosol mixing ratios mostly within 20% of observations, while surface $SO_2$ mixing ratios were overpredicted by factors of two or more [*Barrie et al.*, 2001]. Suggested reasons for the large discrepancy in surface $SO_2$ concentrations include uncertainties in vertical mixing [*Barrie et al.*, 2001] and emission height of $SO_2$ [*deMeij et al.*, 2006] in source regions, and uncertainties in aqueous-phase sulfate production rates [*Kasibhatla et al.*, 1997; *Roelofs et al.*, 2001]. Large uncertainties also exist in the wet scavenging of sulfur species [*Rasch et al.*, 2000; *Roelofs et al.*, 2001; *Rotstayn and Lohmann*, 2002].

[5] Comparisons of observations with global model results suggest that $SO_2$ oxidation is underestimated in winter source regions because of too little cloud or a missing oxidation mechanism [*Barrie et al.*, 2001; *Feichter et al.*, 1996; *Kasibhatla et al.*, 1997]. *Kasibhatla et al.* [1997] found that the addition of a nonphotochemical oxidation pathway for converting $SO_2$ to sulfate in the boundary layer with a pseudo first-order rate constant of $1-2 \times 10^{-6}$ $s^{-1}$ provides the most reasonable method of bringing model $SO_2$ calculations into better agreement with North American (EMEFS) and European (EMEP) measurements. Field studies in polluted environments in winter have suggested that aqueous-phase S(IV) oxidation by oxygen catalyzed by transition metal ions is the dominant sulfate formation pathway [*Jacob et al.*, 1984, 1989; *Jacob and Hoffmann*, 1983].

[6] The oxygen isotopic composition of sulfate aerosols reflects the differing oxidation pathways of secondary sulfate formation [*Savarino et al.*, 2000], and enables quantitative determination of the relative importance of different oxidation pathways leading to sulfate aerosol formation [*Alexander et al.*, 2002, 2005; *Lee and Thiemens*, 2001; *McCabe et al.*, 2006; *Savarino et al.*, 2003]. Recent oxygen isotope measurements of sulfate aerosols collected at Alert, Canada (82.5°N, 62.3°W) indicate that metal-catalyzed oxidation of S(IV) by $O_2$ in the aqueous-phase is significant during winter [*McCabe et al.*, 2006]. Metal-catalyzed S(IV) oxidation is the only known mechanism that can explain the oxygen isotope observations at Alert during winter (nonphotochemically derived source of sulfate with $\Delta^{17}O$ near 0‰) [*McCabe et al.*, 2006]. It has been known for several decades that the transition metals Fe(III) and Mn(II) catalyze the oxidation of S(IV) to sulfate by $O_2$. However, this chemistry is usually omitted in global atmospheric chemistry models because of the large uncertainties in atmospheric dissolved Fe(III) and Mn(II) concentrations [*Graedel et al.*, 1986], and because it is thought to be important only in regionally polluted environments. Here, we include Fe(III)- and Mn(II)-catalyzed S(IV) oxidation by $O_2$ in a global chemical transport model, GEOS-Chem, which includes the oxygen isotope tracers [*Alexander et al.*, 2005]. Details of the metal-catalyzed S(IV) oxidation mechanism in the model are provided in section 5. Using the isotopic measurements in Alert, Canada by *McCabe et al.* [2006] as a constraint, we examine the importance of this oxidation pathway on the global scale.

## 2. Isotopic Constraints on Sulfur Oxidation Pathways

[7] Kinetic and equilibrium processes such as isotopic exchange or diffusion fractionate oxygen isotopes according to the following relation [*Matsuhisa et al.*, 1978].

$$\frac{R^{17}}{R_0^{17}} = \left(\frac{R^{18}}{R_0^{18}}\right)^{0.52} \tag{1}$$

where $R^x = [^xO]/[^{16}O]$ is the isotopic ratio ($x$ = 17 or 18), measured relative to an international reference standard ($R_0^x$). The standard used for oxygen is Standard Mean Ocean Water (SMOW). The relationship (1) is termed mass-dependent fractionation. Any process that does not follow equation (1) is termed mass-independent (or anomalous) fractionation and is characterized by the $\Delta^{17}O$ value where [*Farquhar et al.*, 2000]

$$\Delta^{17}O(‰) = 10^3 \times \left[\left(\frac{R^{17}}{R_0^{17}}\right) - \left(\frac{R^{18}}{R_0^{18}}\right)^{0.52}\right]. \tag{2}$$

For mass-dependent fractionation, $\Delta^{17}O$ = 0‰. Atmospheric $H_2O$ and $O_2$ have $\Delta^{17}O$ at or near 0‰ [*Lyons*, 2001; *Thiemens*, 1999]. OH and $SO_2$ have $\Delta^{17}O$ = 0‰ throughout the troposphere due to isotopic exchange with water vapor [*Dubey et al.*, 1997; *Holt et al.*, 1981], which erases any source-derived isotopic signature.

[8] Both atmospheric $O_3$ and $H_2O_2$ have positive $\Delta^{17}O$ values. Photochemical model calculations by *Lyons* [2001] constrained with laboratory data [*Janssen et al.*, 1999; *Mauersberger et al.*, 1999] indicate $\Delta^{17}O$ = 35‰ for surface $O_3$, increasing to 38‰ at the tropopause. These values are at the upper end of surface measurements (25–35‰) [*Johnston and Thiemens*, 1997; *Krankowsky et al.*, 1995]. Due to potential sampling artifacts from these difficult measurements [*Brenninkmeijer et al.*, 2003], we assume an average tropospheric $\Delta^{17}O$ value for $O_3$ equal to 35‰ based on calculations by *Lyons* [2001]. $H_2O_2$ measurements from rainwater in La Jolla, CA show a range of 1.3–2.2‰ [*Savarino and Thiemens*, 1999] with an average of 1.7‰. The photochemical model calculations by [*Lyons*, 2001] indicate $\Delta^{17}O$ = 0.9–1.8‰ for tropospheric $HO_2$, the precursor of $H_2O_2$, which is consistent with the $H_2O_2$ measurements. Other potential S(IV) oxidants, such as $HNO_4$, $NO_3$ and HOBr/HOCl, are expected to have large $\Delta^{17}O$ values similar to nitrate (20–40‰) because of the influence of $O_3$ in their formation pathways.

[9] Once $SO_2$ forms in the atmosphere through direct emission or oxidation of reduced sulfur species, it quickly ex-

changes its oxygen atoms with abundant water vapor in the atmosphere, erasing any source signature in the oxygen isotopes [*Holt et al.*, 1981]. The $\Delta^{17}O$ value of sulfate is thus dependent only on the oxidation pathway of $SO_2$ to sulfate [*Savarino et al.*, 2000]. We note that the lack of a source signature in the oxygen isotopic composition of sulfate depends on its formation from the oxidation of $SO_2$. It is thought that the majority of sulfate formation originating from the oxidation of DMS proceeds via $SO_2$; however, the importance of DMS oxidation reactions in the aqueous phase that can produce sulfate via another intermediate (e.g., methanesulfonate [*Zhu et al.*, 2006]) remains to be quantified. Whether or not sulfate formation from the oxidation of DMS proceeds via $SO_2$ has implications for the oxygen isotopic composition of sulfate, as other intermediates may or may not equilibrate isotopically with water to erase the source signal.

[10] Laboratory experiments show that a positive $\Delta^{17}O$ in sulfate originates from aqueous-phase oxidation of $SO_2$ by $H_2O_2$ and $O_3$ through simple transfer of the isotopic anomaly from the oxidant to the sulfate product [*Savarino et al.*, 2000]. Assuming $\Delta^{17}O$ values for $H_2O_2$ and $O_3$ equal to 1.7‰ and 35‰ respectively, the product sulfate $\Delta^{17}O$ values are as follows:

$$\mathrm{R2}: HSO_3^- + H_2O_2 \rightarrow \Delta^{17}O_{SO_4^{2-}} = 0.9‰$$
$$\mathrm{R3}: SO_3^{2-} + O_3 \rightarrow \Delta^{17}O_{SO_4^{2-}} = 8.8‰.$$

Other sulfate sources including gas-phase oxidation by OH in the troposphere, metal-catalyzed oxidation by $O_2$, and primary sulfate are mass-dependently fractionated ($\Delta^{17}O = 0$) [*Lee et al.*, 2002; *Savarino et al.*, 2000]. Halogen S(IV) oxidation does not transfer the oxygen from the halogen, but rather promotes the hydrolysis of aqueous sulfate [*Fogelman et al.*, 1989], leading to an expected $\Delta^{17}O = 0‰$ [*McCabe et al.*, 2006]. The $\Delta^{17}O$ value of sulfate formed by $HNO_4$ and $NO_3$ is expected to be similar in magnitude to oxidation by $O_3$ (R3). Sulfate in the atmosphere does not undergo further isotopic exchange.

## 3. Atmospheric Iron (Fe) and Manganese (Mn)

[11] Atmospheric Fe and Mn have both anthropogenic (primarily coal combustion [*Luo et al.*, 2008]) and natural (mineral dust) sources, with the mineral dust source dominant globally [*Salomons and Forstner*, 1984; *Siefert et al.*, 1998]. Concentrations of Mn and Fe in the global atmosphere are highly variable in time and space, ranging from <1 ng $m^{-3}$ to >1,000 ng $m^{-3}$ in the northern hemisphere [*Chen and Siefert*, 2004; *Kubilay and Saydam*, 1995; *Liu et al.*, 2002; *Sedwick et al.*, 2007], with concentrations of Fe typically one order of magnitude greater than Mn [*Baker et al.*, 2006; *Hao et al.*, 2007; *Sedwick et al.*, 2007].

[12] Measurements of the soluble fraction of Fe in the atmosphere vary greatly, from <1% to 80% [*Bonnet and Guieu*, 2004; *Chen and Siefert*, 2003, 2004; *Johansen et al.*, 2000; *Siefert et al.*, 1998; *Spokes et al.*, 1994]. Fractional solubility values on the low end are observed near dust source regions, with higher solubility in more remote or anthropogenic source regions [*Baker et al.*, 2006; *Desboeufs et al.*, 2005; *Hand et al.*, 2004]. Although fractional Fe solubility as high as 80% has been reported [*Chen and Siefert*, 2004], averaged values away from dust source regions are typically between 5–25% [*Baker et al.*, 2006; *Sedwick et al.*, 2007; *Siefert et al.*, 1998]. For comparison, the median solubility of Fe in Saharan dust aerosol was measured to be 1.2% [*Baker et al.*, 2006]. The solubility of Mn (25–100%) tends to be higher than Fe [*Baker et al.*, 2006; *Desboeufs et al.*, 2005; *Deutsch et al.*, 1997; *Hofmann et al.*, 1991; *Siefert et al.*, 1998], with similar fractional solubility in dust, remote and anthropogenic source regions [*Baker et al.*, 2006]. The solubility of both Fe and Mn have been shown to increase with decreasing pH [*Guieu et al.*, 1994; *Mackie et al.*, 2005], and metals from anthropogenic sources are more soluble than metals from natural sources [*Desboeufs et al.*, 2005]. Laboratory experiments show that Fe solubility is a strong function of pH, with highest solubility seen under low pH conditions (pH = 2–3) [*Spokes et al.*, 1994]. Laboratory experiments that increased pH to simulate neutralization by ammonia and crustal materials resulted in almost complete removal of Fe from the solution phase. In contrast, Mn was irreversibly solubilized [*Spokes et al.*, 1994].

[13] The speciation of Fe is important since only Fe(III) can catalyze S(IV) oxidation. Iron in cloud water exists as both Fe(II) and Fe(III), with a series of oxidation and reduction reactions cycling between the two species. Measurements of the fraction of total iron present as Fe(II) show considerable variation, from a few percent to 90% [*Rao and Collett*, 1998, and references therein]. Partitioning between Fe(II) and Fe(III) varies diurnally (from <2% to ~100%) [*Siefert et al.*, 1998], with the highest fraction of Fe(II) found during the day because of photochemical reactions reducing Fe(III) to Fe(II) [*Siefert et al.*, 1998; *Zhu et al.*, 1997].

[14] Mn is mainly present in atmospheric aqueous solutions in the Mn(II) and Mn(III) oxidation states [*Berglund et al.*, 1993]. Thermodynamic calculations [*Deutsch et al.*, 1997; *Hofmann et al.*, 1991] indicate that Mn will exist in equilibrium totally as Mn(II) because of the instability of Mn(III) under atmospheric conditions, except for the possibility of a short-lived Mn(III) intermediate during the S(IV) oxidation mechanism. Laboratory experiments indicated that Mn(III) is a necessary intermediate in the Mn(II)-catalyzed oxidation of S(IV) in aqueous solution, taking place by a free radical mechanism [*Berglund et al.*, 1993].

[15] Large uncertainty exists in the reaction rates of Fe(III)- and Mn(II)-catalyzed S(IV) + $O_2$ [*Hoffmann and Jacob*, 1984; *Martin and Hill*, 1987a], and the reaction is thought to be inhibited by increasing ionic strength, the sulfate ion, various organics, and self-inhibited [*Kotronarou and Sigg*, 1993; *Martin and Hill*, 1987a, 1987b; *Podkrajsek et al.*, 2006; *Tursic et al.*, 2003; *Zuo and Zhan*, 2005]. The presence of both Fe(III) and Mn(II) enhances the reaction rate synergistically, so that the overall reaction rate is greater than the sum of the individual rates [*Berglund et al.*, 1993; *Chughtai et al.*, 1993; *Coichev et al.*, 1992; *Grgic et al.*, 1992; *Martin*, 1984]. Studies of other transition metals such as copper [*Graedel and Weschler*, 1981; *Grgic et al.*, 1991], cobalt [*Bengtsson and Bjerle*, 1975] and nickel [*Graedel and Weschler*, 1981] have been performed; however, Fe and Mn are thought to be the most efficient transition metal

catalysts for S(IV) oxidation [*Berglund et al.*, 1993; *Weschler et al.*, 1986; *Yermakov et al.*, 1997].

## 4. GEOS-Chem Model

[16] We use the GEOS-Chem global 3-D model of coupled aerosol-oxidant chemistry [*Park et al.*, 2004] to simulate the sulfate $\Delta^{17}O$ observations from Alert. The model (version 7.04; see http://www-as.harvard.edu/chemistry/trop/geos/geos_versions.html) uses assimilated meteorological data from the NASA Goddard Earth Observing System (GEOS) including winds, convective mass fluxes, mixed layer depths, temperature, precipitation, and surface properties. Meteorological data have 6-hour temporal resolution (3 hours for surface variables and mixing depths). Meteorological fields have $1^\circ \times 1^\circ$ horizontal resolution with 48 sigma vertical levels (including seven below 1 km for a column based at sea level). For input into GEOS-Chem we degrade the horizontal resolution to $2^\circ \times 2.5^\circ$ ($4^\circ \times 5^\circ$ for the sensitivity simulations) and vertical resolution to 30 sigma vertical levels. The *McCabe et al.* [2006] observations occurred continuously from July 1999–June 2000. We conduct simulations for the year 2001 after a 6-month model spin-up.

[17] The sulfur simulation is as described by *Alexander et al.* [2005]. Sulfate produced by each oxidation pathway is transported as a separate "tracer" in the model with a corresponding $\Delta^{17}O$ value. Total sulfate and $\Delta^{17}O$ are determined locally by addition. Anthropogenic sources of sulfur in the model total 66.1 Tg S year$^{-1}$. This anthropogenic sulfur is emitted as $SO_2$ except for 3% as primary $SO_4^{2-}$ (5% in Europe) [*Chin et al.*, 2000]. Anthropogenic emissions of $SO_x$ in the model is for 1998 and is obtained by scaling the gridded, seasonally resolved inventory from the Global Emissions Inventory Activity (GEIA) for 1985 [*Benkovitz et al.*, 1996]. Natural sources include oceanic phytoplankton (19.6 Tg S year$^{-1}$ as DMS), volcanoes (5.5 Tg S year$^{-1}$ as $SO_2$), and biomass burning (1.2 Tg S year$^{-1}$ as $SO_2$). All emissions are distributed vertically by mass in the local mixed layer.

[18] The simulation includes 19 chemical species transported in the model: dimethyl sulfide (DMS), $SO_2$, sulfate (as seven separate tracers), methanesulfonic acid (MSA), ammonia ($NH_3$), ammonium ($NH_4^+$), particulate nitrate ($NO_3^-$), hydrogen peroxide ($H_2O_2$), sea salt, and dust. The model includes gas-phase oxidation of DMS by OH to form $SO_2$ and methanesulfonic acid (MSA), and DMS oxidation by nitrate radicals ($NO_3$) to form $SO_2$ as described by *Park et al.* [2004] with reaction rates from *DeMore et al.* [1997] and yields of $SO_2$ and MSA from *Chatfield and Crutzen* [1990]. Aqueous-phase reactions of DMS are not included in the model. Sulfate formation from oxidation of $SO_2$ takes place in the gas phase by OH, in alkaline sea-salt aerosols by $O_3$, and in cloud droplets by $H_2O_2$, $O_3$, and $O_2$ (metal catalyzed). Cloud liquid water content is calculated in each cloudy grid box using a temperature-dependent parameterization [*Somerville and Remer*, 1984]. The cloud volume fraction in each grid box is specified by an empirical function of the relative humidity [*Sundqvist et al.*, 1989]. In-cloud oxidation of S(IV) occurs at temperatures above 258 K. A cloud pH of 4.5 is assumed. In-cloud chemistry is sensitive to assumptions about cloud pH and freezing, and in that context the Alert oxygen isotope data are useful in providing support for the transition metal-catalyzed versus $O_3$ oxidation pathways.

[19] To calculate the metal-catalyzed S(IV) oxidation chemistry in cloud water, we use the following rate expression [*Martin and Good*, 1991].

$$\frac{-d[S(IV)]}{dt} = 750[Mn(II)][S(IV)] + 2600[Fe(III)][S(IV)] + 1.0 \times 10^{10}[Mn(II)][Fe(III)][S(IV)] \quad (3)$$

where all concentrations are in units of mole l$^{-1}$. This equation accounts for the synergistic effects of the simultaneous presence of Mn(II) and Fe(III). The simulation of Mn(II) and Fe(III) is described in the following section.

[20] We use monthly mean oxidant (OH, $O_3$, $NO_3$) concentration fields and $H_2O_2$ production rates and photolysis frequencies to calculate oxidation of DMS, $SO_2$ and MSA, and total inorganic nitrate ($HNO_3$(g) plus aerosol $NO_3^-$) concentrations from a coupled aerosol-oxidant simulation as described by *Park et al.* [2004]. Total inorganic nitrate from the coupled aerosol-oxidant simulation is partitioned between the gas and particulate phases using the ISORROPIA thermodynamic equilibrium model (version 1.3) [*Nenes et al.*, 1998]. Nitric acid ($HNO_3$(g)) uptake competes with $SO_2$ uptake for available sea-salt alkalinity which is used to calculate pH-dependent S(IV) + $O_3$ oxidation in sea-salt aerosols as described by *Alexander et al.* [2005].

[21] The simulation of dust aerosol uses a combination of two dust mobilization schemes (GOCART and DEAD) as described by *Fairlie et al.* [2007], resulting in dust emissions and burden of 1689 Tg year$^{-1}$ and 25.8 Tg respectively. Wet deposition of aerosols is as described by *Liu et al.* [2001] and includes contributions from scavenging in convective updrafts, rainout and washout from convective anvils and large-scale precipitation, and return to the atmosphere following re-evaporation. Dry deposition velocities for coarse-mode aerosols (>1 $\mu$m diameter) are computed with the size-dependent scheme of *Zhang et al.* [2001] integrated over each model size bin and accounting for hygroscopic growth as a function of relative humidity [*Gerber*, 1985]. Dry deposition velocities for all other species are computed with a standard resistance-in-series scheme based on *Weseley* [1989] as described by *Wang et al.* [1998].

## 5. Model Simulation of Atmospheric Iron (Fe) and Manganese (Mn)

[22] Since Mn and Fe emissions and concentrations are not directly simulated in the model, we scale their atmospheric concentrations to mineral dust and primary sulfate. We scale soil-derived Fe and Mn concentrations based on observations of the chemical composition of mineral dust. Soil-derived Fe ($[Fe]_{soil}$) is scaled to modeled dust concentrations, assuming Fe represents 3.5% of total dust mass based on average Fe content of the Earth's crust [*Taylor and McLennan*, 1985]. The mineral content of soils varies considerably from place to place [*Claquin et al.*, 1999]. Observations of the Fe content of mineral dust aerosol collected in Barbados (North African dust sources) varied from ~1–4%, with an average of 3.4% [*Zhu et al.*, 1997]. We perform an additional simulation

**Table 1.** Description of Assumptions for Emissions, Solubility Efficiencies, and Speciation of Iron (Fe) and Manganese (Mn) for Each Model Simulation With Metal-Catalyzed S(IV) Oxidation[a]

| Model Simulations | Anthropogenic Fe (Mn) Emissions (Tg year$^{-1}$) | Soil Fe (Mn) Emissions (Tg year$^{-1}$) | Fractional Fe Solubility | Fractional Mn Solubility | Fractional Fe(III) Partitioning | Fractional Mn(II) Partitioning |
|---|---|---|---|---|---|---|
| Base | 0.198 (0.020) | 59.1 (1.2) | 10% (anthropogenic) 1% (soil) | 50% | 10% (sunlight) 90% (no sun) | 100% |
| High anthropogenic | 0.660 (0.066) | 59.1 (1.2) | 10% (anthropogenic) 1% (soil) | 50% | 10% (sunlight) 90% (no sun) | 100% |
| Low dust | 0.198 (0.020) | 16.9 (0.3) | 10% (anthropogenic) 1% (soil) | 50% | 10% (sunlight) 90% (no sun) | 100% |
| High Fe solubility | 0.198 (0.020) | 59.1 (1.2) | 25% (anthropogenic) 1% (soil) | 50% | 10% (sunlight) 90% (no sun) | 100% |
| High Mn solubility | 0.198 (0.020) | 59.1 (1.2) | 10% (anthropogenic) 1% (soil) | 100% | 10% (sunlight) 90% (no sun) | 100% |

[a]All sensitivity studies were conducted at 4° × 5° horizontal resolution and 30 vertical layers.

assuming Fe represents just 1% of total dust mass to explore the sensitivity of metal-catalyzed S(IV) oxidation to our assumed dust-scale factor (see Table 1). Observations of the Fe/Mn ratio in mineral dust samples ranged from 14 (Arizona dust) to 59 (Sahara dust) [*Desboeufs et al.*, 2005]. The Saharan dust Fe/Mn ratio [*Desboeufs et al.*, 2005] is similar to the average Fe/Mn ratio of the Earth's crust (Fe/Mn = 58) [*Taylor and McLennan*, 1985]. We scale soil-derived Mn ($[Mn]_{soil}$) as a factor of 50 lower than $[Fe]_{soil}$.

[23] Anthropogenic metals ($[Mn]_{anthro}$ and $[Fe]_{anthro}$) are scaled to primary anthropogenic sulfate ($[SO_4]_{primary}$) because of their similar sources (primarily coal combustion) and sinks (wet and dry deposition). Anthropogenic Mn ($[Mn]_{anthro}$) is scaled to primary anthropogenic sulfate ($[SO_4]_{primary}$) based on estimates of $[Mn]_{anthro}$ concentrations in Alert and Iceland (63°N, 20°W) utilizing the relationship between Mn and Al concentrations in soil at Alert, Canada ($[Mn]_{soil}/[Al]_{soil} = 0.0065$) [*Sirois and Barrie*, 1999]. We chose these locations because of their availability of both Mn and Al aerosol observations year round (unfortunately simultaneous measurements of aerosol Mn and Al closer to source regions are not available). Concentrations of anthropogenic Mn were determined by subtracting out the soil component ($[Mn]_{anthro} = [Mn] - 0.0065[Al]_{soil}$) [*Sirois and Barrie*, 1999]. Our assumption that $[Fe]_{soil} = 50[Mn]_{soil}$ results in the relationship: $[Fe]_{soil}/[Al]_{soil} = 0.325$. For comparison, the Fe/Al ratio in dust aerosols from various regions (Sahara, Asia and Amazonia) ranges from 0.30–0.72, with Sahara dust on the lower end of this range [*Formenti et al.*, 2001; *Guo et al.*, 2002; *Mahowald et al.*, 2005]. The soil contribution of Mn dominates in Alert (91% annual average, 64–99% range), while the anthropogenic contribution tends to dominate in Iceland (62% annual average, 32–77% range). The ratio of modeled $[SO_4]_{primary}$ to measured $[Mn]_{anthro}$ varies over two orders of magnitude (2–300). We make a conservative estimate of modeled $[Mn]_{anthro}$ by using the ratio at the high end of this range ($[SO_4]_{primary}/[Mn]_{anthro} = 300$). Anthropogenic Fe ($[Fe]_{anthro}$) is assumed to be 10 times that of $[Mn]_{anthro}$ based on observations of atmospheric fly-ash particles [*Desboeufs et al.*, 2005].

[24] *Luo et al.* [2008] did a more sophisticated treatment of combustion sources of iron in a global model by estimating emissions from both industrial and biomass combustion in size-segregated aerosols. Their industrial source estimate was based on literature values of mineral matter emission factors and a model of global combustion sources [*Bond et al.*, 2004]. Since the goal of their paper was to assess whether combustion sources of iron are potentially important, they used high-end estimates of industrial Fe emission factors. Coal combustion dominated the industrial source of iron (>75%) which is concentrated in East Asia, Europe and the east coast of North America. The biomass burning source was estimated on the basis of observed ratios of iron to black carbon in the Amazon [*Fuzzi et al.*, 2007] and is concentrated in tropical regions. Although we neglect the biomass burning source of Fe and Mn, we don't expect this to play an important role in S(IV) oxidation because of the predominantly tropical location of emissions, where photochemical oxidation (by OH and $H_2O_2$) of S(IV) dominates year round. Their industrial source of Fe (0.663 Tg year$^{-1}$) is over 3 times larger than ours (0.198 Tg year$^{-1}$). We perform a sensitivity study increasing our anthropogenic emissions of metals to be similar to that of *Luo et al.* [2008] by using a scale factor of $[SO_4]_{primary}/[Mn]_{anthro} = 90$ in order to explore the sensitivity of metal-catalyzed S(IV) oxidation to our assumed anthropogenic metal emission factors (see Table 1). Their estimated uncertainty of combustion Fe emissions (industrial and biomass) is a factor of 4–5, with the largest uncertainty from coal combustion due partly to the sensitivity to poorly known emission control technologies. Their comparison of simulated total (combustion and dust) Fe with observations in Cheju, Korea (33.5°N, 126.5°E) reveals a low bias; however, the dust source is predicted to dominate in this location most of the year. For comparison, their dust source of Fe (54.8 Tg year$^{-1}$) is similar to ours (59.1 Tg year$^{-1}$).

[25] Figure 1 (top and middle) shows annual average calculated $[Mn]_{soil}$ and $[Mn]_{anthro}$ at the surface for our base simulation (see Table 1 for a description of the model simulations). The mineral dust source dominates atmospheric Mn and Fe concentrations on the global scale. $[Fe]_{soil}$ is 50 times higher than $[Mn]_{soil}$, and $[Fe]_{anthro}$ is 10 times higher than $[Mn]_{anthro}$ (not shown). The anthropogenic source dominates (>50%) in regions of high anthropogenic emissions and small dust sources such as eastern North America and parts of central and western Europe (Figure 1, bottom).

[26] We compare simulated Mn and Fe concentrations with observations in a remote region (Alert), anthropogenic source regions (Europe and China), and near a major dust source (Gobi desert). Figure 2 compares observations of total Mn ($[Mn]_{total}$), anthropogenic Mn ($[Mn]_{anthro}$), soil Mn ($[Mn]_{soil}$), and soil fraction ($[Mn]_{soil}/[Mn]_{total}$) at Alert, along with model calculations. The observations are plotted as monthly means, with the error bars representing the full range of measurements during that month. $[Mn]_{total}$ calculations fall within the range of observations for all months of the year except for a slight overestimate in March. Calculations of $[Mn]_{anthro}$ underestimate observations January–May, and are at the low end of the range of observations for the rest of the year. $[Mn]_{soil}$ calculations fall within the range of

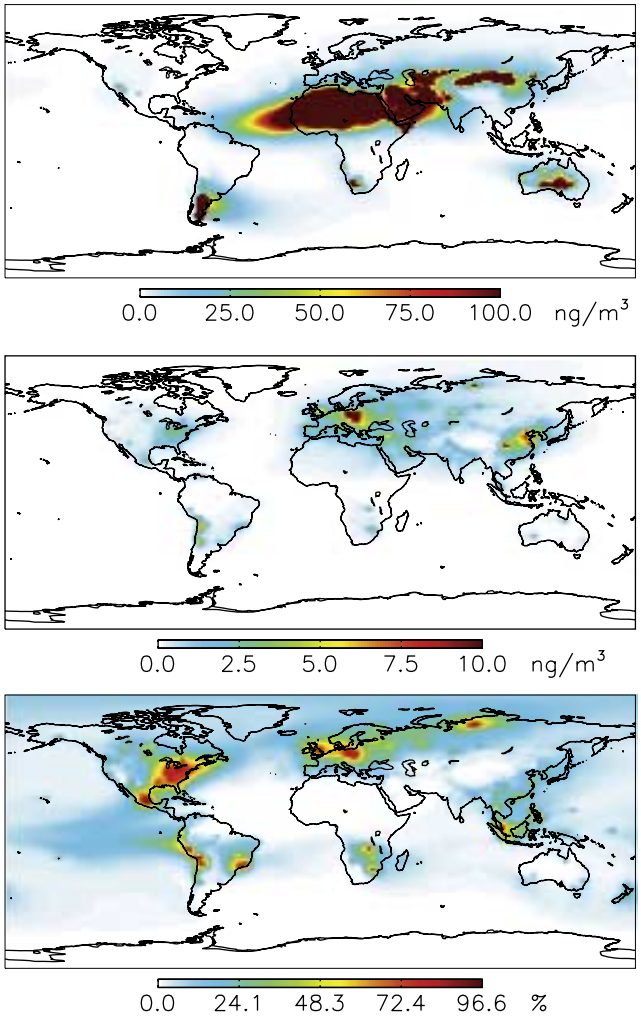


**Figure 1.** Modeled annual mean global (top) natural and (middle) anthropogenic Mn concentrations (ng $m^{-3}$) at the surface, along with the percent of anthropogenic Mn compared to total Mn concentrations (bottom).

observations for all months, except for a slight overestimate in March. $[Mn]_{soil}$ dominates total Mn concentrations in both the observations and model simulations, particularly during summer, but the model overestimates the soil fraction year round.

[27] Our sensitivity study with a high-end anthropogenic metal emissions factor similar to *Luo et al.* [2008] also gives good agreement with observed $[Mn]_{total}$ at Alert, similar to our base simulation. Comparison with $[Mn]_{anthro}$ shows that our simulation with high anthropogenic emissions tends to underestimate observations of $[Mn]_{anthro}$ at Alert, though less so than our base simulation (11–87% underestimate, compared to 70–94% for our base simulation). In contrast to our base simulation, the high anthropogenic simulation tends to underestimate the soil fraction except during spring (MAM). The sensitivity simulation using lower emissions of dust-derived metals underestimates observations of $[Mn]_{soil}$ at Alert by 33–98%, and underestimates the soil fraction by 5–65% except during spring (20–70% overestimate).

[28] Table 2 compares seasonal-mean modeled Mn and Fe with observations at European EMEP sites where Mn and/or Fe observations are available (n = 17 and n = 5 sites, respectively), and in a coastal suburban (Qindao) and desert (Minqin) location in China. The model tends to overestimate both Mn and Fe at the EMEP sites (which are all in central and northern Europe) by a factor of 1.4–2.7. The anthropogenic fraction of Mn and Fe tends to dominate (generally >50%) at these EMEP sites, suggesting an overestimate of

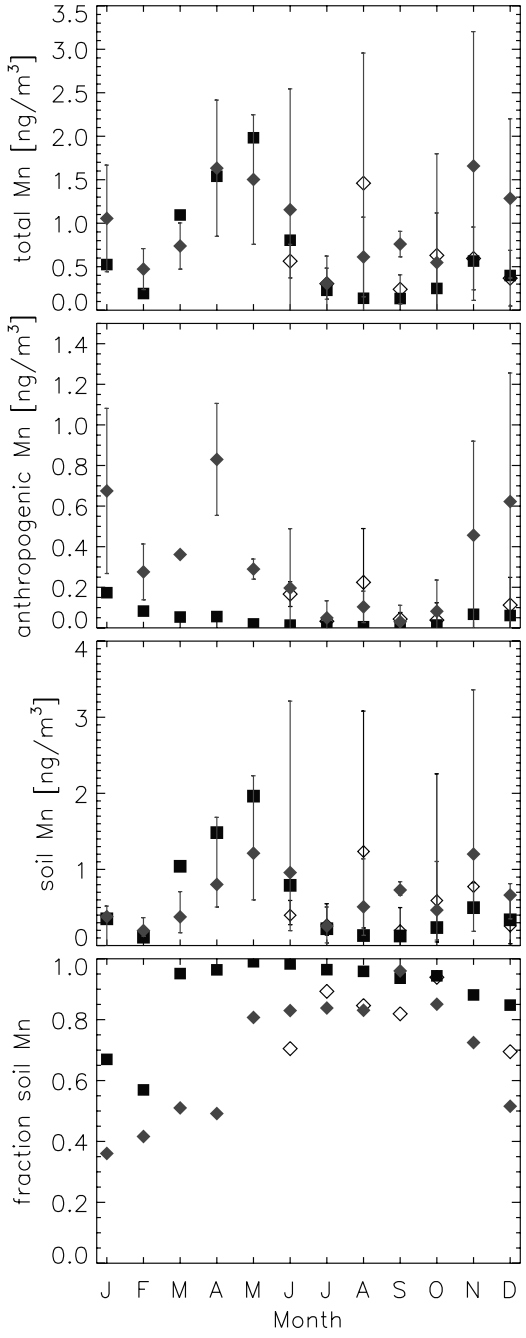


**Figure 2.** Monthly mean total, anthropogenic, and soil Mn concentrations for the model (solid squares) compared to observations from the year 2000 (open diamonds) and 2001 (gray diamonds) at Alert, Canada. The error bars on the observations represent the total range of observations for each month. Also shown is the soil fraction of total Mn concentrations for 2001.

**Table 2.** Comparison of Observed and Modeled Seasonal Mean Mn and Fe Concentrations (ng $m^{-3}$) From European EMEP Sites and a Suburban (Qindao) and Desert (Minqin) Site in China

| | Fe (Mn) Observations (ng $m^{-3}$) | Fe (Mn) Model (ng $m^{-3}$) | Fe (Mn) Model/Observations | Reference |
|---|---|---|---|---|
| EMEP (central and northern Europe) | | | | www.emep.int |
| Spring | 82.8 (3.9) | 126.1 (806) | 1.5 (2.2) | |
| Summer | 67.4 (3.7) | 67.4 (5.3) | 1.5 (1.4) | |
| Autumn | 72.5 (4.4) | 72.5 (8.8) | 2.7 (2.0) | |
| Winter | 65.8 (4.3) | 96.4 (9.5) | 1.5 (2.2) | |
| Minqin, China (35.6°N, 103.1°E) | | | | *Liu et al.* [2002] |
| Spring | 3600.0 (79.0) | 6725.8 (135.0) | 1.7 (1.9) | |
| Summer | 2900.0 (63.0) | 1728.3 (35.0) | 0.60 (0.56) | |
| Qindao, China (35.4°N, 120.2°E) | | | | *Hao et al.* [2007] |
| Spring | 2880.0 (65.8) | 2706.9 (58.5) | 0.94 (0.89) | |
| Summer | 1541.3 (44.4) | 253.3 (8.0) | 0.16 (0.18) | |
| Autumn | 2996.8 (72.0) | 876.4 (21.3) | 0.29 (0.30) | |
| Winter | 3788.1 (133.5) | 185.8 (8.8) | 0.05 (0.07) | |

anthropogenic metals in this region. Model comparison with observations in Qindao [*Hao et al.*, 2007] shows good agreement in spring (within ~10% for both Mn and Fe), with model calculations underestimating the observations during the rest of the year. Spring is the only time of year when the anthropogenic component of metals does not dominate at this location in the model, suggesting an underestimate of anthropogenic metal emission rates in this region. Our simulation with higher anthropogenic emission factors similar to *Luo et al.* [2008] also underestimates Mn (Fe) in Qindao by a factor of 0.2–0.5 (0.1–0.3), except during spring (10–20% overestimate). The simultaneous overestimate in Europe and underestimate in suburban China highlights the limitations of our approach applying a global-scale factor of $[SO_4]_{primary}/[Mn]_{anthro}$, as regionally varying emissions control technologies may impact the relative emission rates. The regionally varying discrepancies may also be due in part to an outdated emissions inventory. Model comparison with observations in Minqin [*Liu et al.*, 2002] indicate that the model overestimates Mn and Fe by a factor of 2.2 and 2.3 respectively during spring, and underestimates by 50% for both species during summer. The dust source dominates (~99%) in this location during both spring and summer in the model. Our sensitivity simulation with lower dust emissions underestimates Mn (Fe) in Minqin by a factor of 0.1 and 0.6 (0.1 and 0.7) in summer and spring, respectively.

[29] The solubility and speciation of Fe and Mn is important for S(IV) oxidation. If cloud liquid water is available, we assume that 50% of $[Mn]_{total}$ is dissolved in cloud water, which is within the range (25–100%) of available observations [*Baker et al.*, 2006; *Desboeufs et al.*, 2005; *Deutsch et al.*, 1997; *Hofmann et al.*, 1991; *Siefert et al.*, 1998]. We assume that 100% of the dissolved Mn is in the Mn(II) oxidation state based on thermodynamic calculations by *Deutsch et al.* [1997] and *Hofmann et al.* [1991]. For Fe, we assume that 10% of $[Fe]_{anthro}$ and 1% of $[Fe]_{soil}$ is dissolved if cloud liquid water is available (similar to *Bopp et al.* [2003], *Fung et al.* [2000], and *Wu and Boyle* [2002]). We use a solubility fraction of 1% for $[Fe]_{soil}$ based on measurements of the median solubility (1.2%) of Fe in Saharan dust aerosol [*Baker et al.*, 2006]. The choice of 10% for $[Fe]_{anthro}$ is based on the higher solubility of Fe from anthropogenic activities compared to that in mineral dust, and is within the typical range of 5–25% observed away from dust source regions [*Baker et al.*, 2006; *Sedwick et al.*, 2007; *Siefert et al.*, 1998]. We also perform two simulations assuming higher solubility efficiencies (100% and 25% for Mn and anthropogenic Fe, respectively) to test the sensitivity of metal-catalyzed S(IV) oxidation to our solubility assumptions (see Table 1). The oxidation state of dissolved Fe depends on sunlight. If there is sunlight, 10% of dissolved Fe is in the Fe(III) oxidation state. If there is no sunlight, 90% of Fe is in the Fe(III) oxidation state. The partitioning between Fe(II) and Fe(III) is based on the observed range of the Fe(II) fraction (<2–~100%), and the diurnal cycling favoring Fe(III) at night [*Siefert et al.*, 1998].

[30] Calculated concentrations of annual mean dissolved Mn(II) and Fe(III) have a very large range (0–10 $\mu$M), but are mostly between 0.1–1 $\mu$M (0.01–0.1 $\mu$M) in the Northern Hemisphere (Southern Hemisphere) boundary layer (<2-km altitude). Measurements of soluble Mn in fog and rainwater at sites on the east and west coasts of the U.S. and in Germany range from ~0.0002–0.2 $\mu$M [*Deutsch et al.*, 1997; *Hofmann et al.*, 1991; *Siefert et al.*, 1998]. Soluble Fe concentrations in rainwater from Germany were ~0.5 $\mu$M [*Hofmann et al.*, 1991]. Very few speciated measurements are available, and such measurements are uncertain due in part to the difficulties associated with isolating the species of interest from complex matrices, and that most of the speciation techniques available disturb the equilibria existing between various chemical species [*Pickering*, 1996]. Most studies report observations of Fe(II), not Fe(III) [*Behra and Sigg*, 1990; *Siefert et al.*, 1998; *Zhu et al.*, 1997; *Zhuang et al.*, 1992a, 1992b, 1995]. Observations of Fe(III) range from 0–9 $\mu$M at locations mostly in the Los Angeles area [*Erel et al.*, 1993; *Pehkonen et al.*, 1992; *Rao and Collett*, 1998].

## 6. Model Evaluation of Metal-Catalyzed S(IV) Oxidation in Alert, Canada

[31] Figure 3 (top) shows monthly mean nss$SO_4^{2-}$ $\Delta^{17}O$ observations [*McCabe et al.*, 2006] and model calculations at Alert, Canada. Model calculated values from a simulation with no transition metal chemistry (gray squares) consistently overestimate the $\Delta^{17}O$ values, by a factor of 3 during winter and a factor of 2 during summer. The large $\Delta^{17}O$ values calculated during winter result from S(IV) oxidation by $O_3$, similar to *Feichter et al.* [1996]. S(IV) oxidation by $O_3$

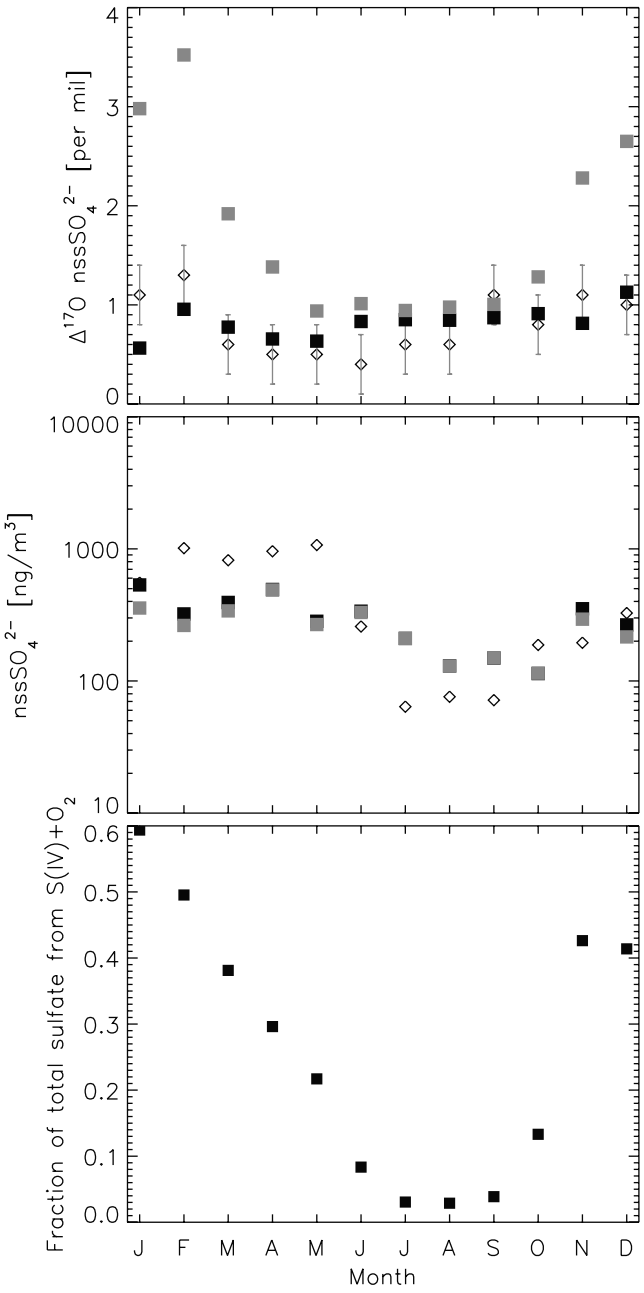


**Figure 3.** Monthly mean observations (open diamonds with shaded error bars) and model calculations in Alert, Canada, from the model simulation with no metal-catalyzed S(IV) oxidation (gray squares) and the simulation with metal-catalyzed S(IV) oxidation (solid squares). (top) $nssSO_4^{2-}$ $\Delta^{17}O$ [‰]. (middle) $nssSO_4^{2-}$ concentrations [ng m$^{-3}$]. (bottom) Fraction of total sulfate from the metal-catalyzed S(IV) + $O_2$ oxidation pathway.

dominates during winter in the model because of low OH and $H_2O_2$ concentrations resulting from the lack of sunlight. Including metal-catalyzed S(IV) oxidation in the model significantly lowers the calculated $\Delta^{17}O$ values in winter, and has a negligible effect in summer. The calculated $\Delta^{17}O$ values generally fall within the uncertainty in the observations, except for a tendency to overestimate by ~0.5‰ (factor of 2) during summer.

[32] The sulfate $\Delta^{17}O$ calculations from the sensitivity study using high-end anthropogenic metal emission rates similar to *Luo et al.* [2008] tend to underestimate the observed $\Delta^{17}O$ values during winter by 0.5‰ (~0.4‰ lower than our base simulation). Our simulation using a Fe dust mass fraction of 1% shows no significant change in calculated sulfate $\Delta^{17}O$ values at Alert compared to our base simulation (less than 0.2‰ difference), suggesting that anthropogenic metals dominate metal-catalyzed S(IV) oxidation in this region. Likewise, our sensitivity simulations using higher solubility efficiencies for Fe and Mn result in $\Delta^{17}O$ values similar to our base simulation (less than 0.2‰ difference), suggesting that the largest uncertainty in our estimates of metal-catalyzed S(IV) oxidation in this region is from unknown anthropogenic metal emission rates.

[33] Figure 3 (middle) shows monthly mean sulfate concentration observations and model calculations for the year 2001 at Alert, Canada. All model simulations reproduce the observed seasonality with concentrations higher in winter than in summer. The strong seasonality of aerosol concentrations in the Arctic is due to the intensification of meridional transport from the midlatitudes during winter and spring [*Iversen and Joranger*, 1985; *Quinn et al.*, 2007]. In addition, stable thermal stratification in the boundary layer and low precipitation during winter months leads to significantly longer atmospheric residence times from October to May [*Sirois and Barrie*, 1999]. All simulations tend to underestimate (overestimate) sulfate concentrations in winter (summer), with slightly better agreement during winter for the simulations with metal-catalyzed oxidation of S(IV).

[34] Figure 3 (bottom) shows model calculated monthly mean fractions of total sulfate formed by the metal-catalyzed oxidation pathway at Alert, Canada. Sulfate formed via the metal catalysis pathway dominates (~40–60%) total sulfate at Alert during winter (~50–70% using anthropogenic emission factors similar to *Luo et al.* [2008]). *McCabe et al.* [2006] estimated a 10–18% contribution from the metal-catalyzed oxidation pathway during winter. Their estimate is biased low because they are comparing their measurements with global model results averaged north of 40°N latitude [*Feichter et al.*, 1996], which will underestimate the relative contribution of ozone as a S(IV) oxidant locally at Alert. Summertime fractions are low (<10% for all simulations).

## 7. Impacts on the Global Sulfur Budget

[35] Table 3 shows the global atmospheric burden (Tg S), lifetime (days), and loss frequency (day$^{-1}$) of $SO_2$ and sulfate for the model simulations with and without metal-catalyzed S(IV) + $O_2$ chemistry, along with the importance of each sulfate production pathway (Tg S year$^{-1}$). Metal-catalyzed oxidation of S(IV) decreases the $SO_2$ burden by 7–12% globally by increasing aqueous-phase oxidation and thus decreasing its lifetime. In-cloud oxidation by $H_2O_2$ dominates atmospheric sulfate production in all simulations. Metal-catalyzed S(IV) oxidation accounts for 9–17% of total sulfate production globally. Total in-cloud sulfate production increases by 3–6%, to account for 56–59% of total sulfate production. The global atmospheric sulfate burden increases by <10% for each simulation.

[36] Figure 4 shows the annual mean fraction of total sulfate at the surface formed through metal-catalyzed oxida-

**Table 3.** Comparison of Sulfur Budgets From the GEOS-Chem Model Simulations (4° × 5° Horizontal Resolution) With and Without Metal-Catalyzed S(IV) + $O_2$ Chemistry

| Budget Component | No Metal Catalysis Chemistry | | Metal Catalysis Chemistry[a] Base | | High Anthropogenic | | Low Dust | | High Fe Solubility | | High Mn Solubility | |
|---|---|---|---|---|---|---|---|---|---|---|---|---|
| Burden, Tg S | | | | | | | | | | | | |
| $SO_2$ | 0.33 | | 0.30 | | 0.29 | | 0.30 | | 0.30 | | 0.30 | |
| Sulfate | 0.36 | | 0.38 | | 0.39 | | 0.37 | | 0.39 | | 0.39 | |
| Lifetime, days | | | | | | | | | | | | |
| $SO_2$ | 1.38 | | 1.26 | | 1.22 | | 1.28 | | 1.24 | | 1.24 | |
| Sulfate | 3.30 | | 3.32 | | 3.29 | | 3.30 | | 3.31 | | 3.32 | |
| Loss frequency[b], $day^{-1}$ | | | | | | | | | | | | |
| $SO_2$ dry deposition | 0.29 | | 0.30 | | 0.30 | | 0.30 | | 0.30 | | 0.30 | |
| $SO_2$ in-air oxidation | 0.07 | | 0.07 | | 0.07 | | 0.07 | | 0.07 | | 0.07 | |
| $SO_2$ wet processes[c] | 0.36 | | 0.42 | | 0.44 | | 0.41 | | 0.43 | | 0.43 | |
| Sulfate dry deposition | 0.07 | | 0.07 | | 0.07 | | 0.07 | | 0.07 | | 0.07 | |
| Sulfate wet deposition | 0.23 | | 0.23 | | 0.23 | | 0.23 | | 0.23 | | 0.23 | |
| Sulfate production, Tg S $year^{-1}$ | | | | | | | | | | | | |
| Gas phase (OH) | 8.3 | (22%) | 8.1 | (21%) | 8.0 | (20%) | 8.1 | (21%) | 8.0 | (20%) | 8.0 | (20%) |
| In-cloud ($H_2O_2$) | 18.9 | (51%) | 17.5 | (44%) | 16.8 | (41%) | 18.0 | (46%) | 17.2 | (43%) | 17.2 | (43%) |
| In-cloud ($O_3$) | 0.8 | (2%) | 0.5 | (1%) | 0.3 | (1%) | 0.5 | (1%) | 0.4 | (1%) | 0.4 | (1%) |
| Sea-salt ($O_3$) | 9.1 | (25%) | 8.7 | (22%) | 8.6 | (21%) | 8.7 | (23%) | 8.6 | (22%) | 8.6 | (21%) |
| In-cloud ($O_2$) | 0.0 | (0%) | 4.8 | (12%) | 7.1 | (17%) | 3.6 | (9%) | 5.7 | (14%) | 5.8 | (15%) |
| Total in-cloud | 19.7 | (53%) | 22.8 | (57%) | 24.2 | (59%) | 22.1 | (56%) | 23.3 | (58%) | 23.4 | (59%) |
| Total sulfate | 37.2 | | 39.6 | | 40.8 | | 38.8 | | 40.0 | | 40.1 | |

[a]See Table 1 for a description of each simulation.
[b]Loss frequency is defined as the loss rate divided by the burden.
[c]Including in-cloud oxidation and wet scavenging.

tion. Sulfate formed through metal catalysis represents up to 48% of total sulfate on an annual mean basis, with the highest fraction over the polluted industrial regions of northern Eurasia. Sulfate formed through metal-catalyzed oxidation accounts for ~25% of total sulfate downwind of the Sahara desert. Metal catalysis chemistry is important in higher latitudes because of the decreased importance of photochemical reactions in winter compared to lower latitudes.

[37] Figure 5 shows the annual mean percent decrease (increase) in $SO_2$ (sulfate) concentrations summed over the boundary layer (<2-km altitude) after including the metal catalysis chemistry. The addition of metal-catalyzed S(IV) oxidation decreases $SO_2$ concentrations by ~50% in the Arctic (>60°N latitude). Sulfate concentrations increase by up to 20% in the Arctic and near anthropogenic and dust

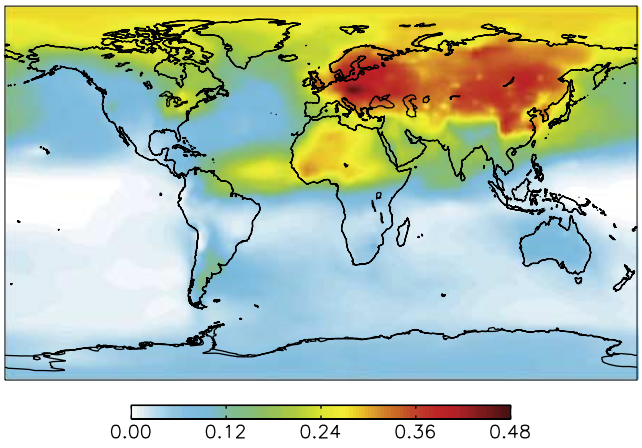


**Figure 4.** Annual mean fraction of total sulfate at the surface from the metal-catalyzed S(IV) + $O_2$ oxidation pathway.

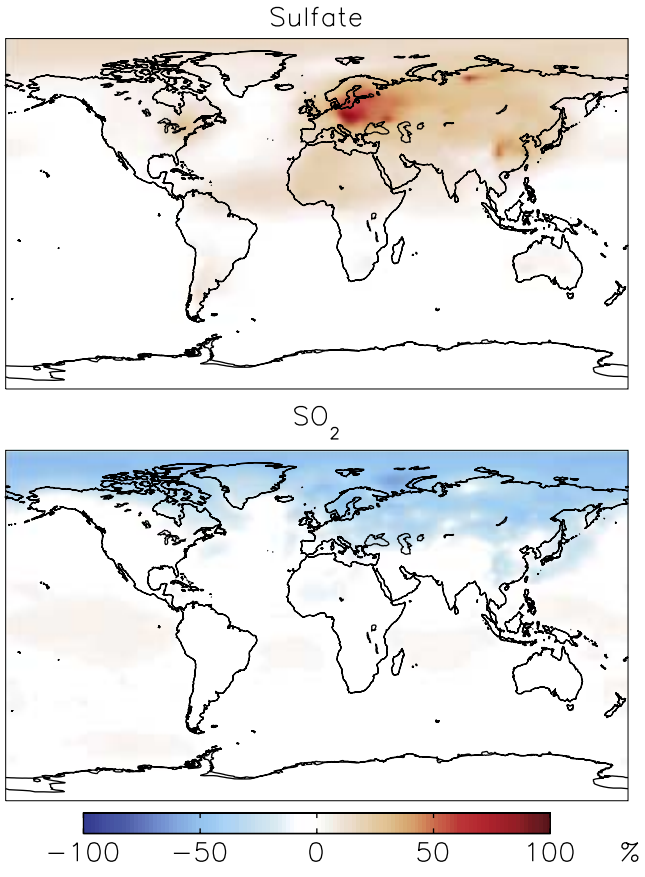


**Figure 5.** Percent decrease (increase) in $SO_2$ (sulfate) concentrations in the boundary layer (<2-km altitude) after adding metal-catalyzed S(IV) oxidation to the model.

**Table 4.** Comparison of Seasonal-Mean Observed and Modeled $SO_2$ and Non–Sea-Salt $SO_4^{2-}$ Concentrations ($\mu g\ m^{-3}$) at European EMEP Sites (www.emep.int)

| | $SO_2$ ($SO_4^{2-}$) Observations ($\mu g\ m^{-3}$) | $SO_2$ ($SO_4^{2-}$) Model ($\mu g\ m^{-3}$) | $SO_2$ ($SO_4^{2-}$) Model/Observations |
|---|---|---|---|
| *Model with no metal-catalyzed S(IV) oxidation* | | | |
| Spring | 1.51 (2.15) | 6.26 (3.41) | 4.1 (1.6) |
| Summer | 1.13 (2.46) | 3.25 (3.49) | 2.9 (1.4) |
| Autumn | 1.36 (1.94) | 6.37 (2.80) | 4.7 (1.4) |
| Winter | 2.52 (1.95) | 11.88 (2.25) | 4.7 (1.2) |
| *Model with metal-catalyzed S(IV) oxidation* | | | |
| Spring | 1.51 (2.15) | 5.42 (4.60) | 3.6 (2.1) |
| Summer | 1.13 (2.46) | 3.19 (3.62) | 2.8 (1.5) |
| Autumn | 1.36 (1.94) | 5.33 (4.10) | 3.9 (2.1) |
| Winter | 2.52 (1.95) | 8.72 (6.09) | 3.5 (3.1) |

source regions (most of Eurasia and Northern Africa, northeastern North America, and the northern subtropical Atlantic). The largest increase (~100%) occurs over central Europe (Czech Republic, Slovakia, and Hungary). Since the largest increase in sulfate concentrations occurs over Europe, we compare our simulations with EMEP $SO_2$ and sulfate observations for the year 2001, which are located primarily in Western Europe.

[38] Table 4 compares seasonal mean EMEP $SO_2$ and sulfate surface concentrations for the year 2001 to the model simulations with and without metal catalysis. As with most models, the model overestimates $SO_2$ concentrations during all seasons with and without metal-catalyzed S(IV) oxidation. The simulation with no metal catalysis overestimates $SO_2$ by a factor of 2.9–4.7, with a maximum overestimate in autumn and winter. The simulation with metal catalysis chemistry has a slightly smaller overestimate of $SO_2$ over all seasons (factor of 2.8–3.9 with maximum overestimate during autumn). Calculated sulfate concentrations for the simulation with no metal catalysis chemistry overestimate the observations by 20–60%. The base simulation with metal catalysis chemistry overestimates sulfate observations by a factor of 1.5–3.1, with the maximum overestimate during winter.

[39] As mentioned above, *Kasibhatla et al.* [1997] found that the addition of a nonphotochemical oxidation pathway for converting $SO_2$ to sulfate in the boundary layer with a pseudo (spatially and temporally constant) first-order rate constant of $1–2 \times 10^{-6}\ s^{-1}$ provides the most reasonable method of bringing model results into better agreement with surface observations of $SO_2$ in Europe and North America. They suggested that this reaction could occur on the surface of aerosols and in fog droplets. Our first-order rate constant is highly variable in space and time, as it is dependent upon concentrations of Mn(II) and Fe(III) and the availability of cloud liquid water. Our annual average first-order rate constant for the metal-catalyzed oxidation of S(IV) is a maximum on the order of $10^{-4}\ s^{-1}$ downwind of the Sahara desert. Over Europe and Asia, the reaction rate varies over three orders of magnitude in winter ($10^{-7}$ to $10^{-4}$) with maximum values in central Europe and Asia, and is negligible in summer. Outside of Eurasia, parts of the Middle East and downwind of the Sahara desert, the reaction rate is negligible year-round. Despite localized first-order reaction rate constants as high as $10^{-4}\ s^{-1}$ in source regions during winter, the inclusion of metal catalysis chemistry does not fully reconcile the discrepancy with European $SO_2$ concentration measurements.

## 8. Conclusions

[40] We used the GEOS-Chem global chemical transport model to quantify transition metal-catalyzed S(IV) oxidation using the *McCabe et al.* [2006] sulfate $\Delta^{17}O$ observations in Alert, Canada, and place them in a global context. We find that our model simulation including metal-catalyzed S(IV) oxidation reconciles the discrepancy between observed and modeled wintertime $\Delta^{17}O$ sulfate in Alert, Canada [*McCabe et al.*, 2006]. Our model results indicate that this reaction pathway may be of global-scale importance, representing 9–17% of annual-mean sulfate production in the present-day atmosphere, with the highest fraction observed over Northern Eurasia. Although natural (dust) sources dominate atmospheric Fe and Mn concentrations, metal-catalyzed oxidation of S(IV) is highest near mid-to-high-latitude anthropogenic sources of these metals because of much lower competition from photochemical reactions during winter.

[41] We applied the GEOS-Chem model to quantify the impact of metal-catalyzed S(IV) oxidation on the atmospheric sulfur budget. We find that this reaction decreases global $SO_2$ concentrations by 9–12%, and results in localized sulfate concentration increases up to 100%. This improves agreement with surface $SO_2$ observations in Europe, but does not fully reconcile the large overestimate of modeled $SO_2$ concentrations, a problem common to most large-scale models of the sulfur cycle [*Barrie et al.*, 2001]. Adding metal-catalyzed S(IV) oxidation to the model results in a large overestimate (factor of 3.1) of EMEP observations of surface sulfate concentrations during winter. Global model comparisons have indicated a large sensitivity of surface $SO_2$ and sulfate concentrations to vertical mixing and emission height of aerosol precursor gases in source regions [*Barrie et al.*, 2001; *deMeij et al.*, 2006], and to wet scavenging efficiencies [*Rasch et al.*, 2000; *Roelofs et al.*, 2001; *Rotstayn and Lohmann*, 2002]. Uncertainties in these processes may be the main source of the discrepancy between modeled and observed $SO_2$. Although oxygen isotopic evidence indicates that metal-catalyzed S(IV) oxidation represents a substantial (up to 48% annual mean) fraction of sulfate in the northern hemisphere mid-to-high latitudes, it does not reconcile the discrepancies with surface $SO_2$ and sulfate concentration measurements in this region.

[42] Emission rates of Fe and Mn, as well as their dissolution rate and oxidation state, are highly uncertain. The largest uncertainty in our ability to quantify the importance of metal-catalyzed S(IV) oxidation lies in unknown anthropogenic metal emission rates, highlighting the need for improved understanding of emission rates of metals from combustion sources. Oxygen isotope measurements of sulfate aerosols collected near metal source regions, such as northern and central Eurasia and downwind of the Sahara desert, are needed to verify the importance of this metal-catalyzed S(IV) oxidation pathway. Additional oxidation pathways not included in the model, such as S(IV) oxidation by $O_3$ on alkaline dust aerosols [*Bauer and Koch*, 2005; *Usher et al.*, 2003] or oxidation by halogens [*Vogt et al.*, 1996], would

further decrease global atmospheric $SO_2$ concentrations, and can be similarly quantified using $\Delta^{17}O$ measurements.

[43] Arctic ice-core sulfate $\Delta^{17}O$ measurements from Greenland extending through the last ~300 years show values in the range of 0.7–3.3‰ [*Alexander et al.*, 2004]. The recent (past ~100 years) decreasing trend in sulfate $\Delta^{17}O$ from this ice core can at least partially be explained by the increasing importance of the metal-catalyzed S(IV) oxidation pathway due to anthropogenic Mn and Fe emissions. Interpretation of these ice-core data with a global 3-D paleoclimate model could provide new information on past trends and anthropogenic impacts on sulfur and oxidant budgets.

[44] **Acknowledgments.** Financial support for this project was provided by grants NSF-ATM 0607846 and NSF-ATM 0704169 to B. Alexander.

## References


Alexander, B., J. Savarino, N. I. Barkov, R. J. Delmas, and M. H. Thiemens (2002), Climate driven changes in the oxidation pathways of atmospheric sulfur, *Geophys. Res. Lett.*, *29*(14), 1685, doi:10.1029/2002GL014879.

Alexander, B., J. Savarino, K. J. Kreutz, and M. H. Thiemens (2004), Impact of preindustrial biomass-burning emissions on the oxidation pathways of tropospheric sulfur and nitrogen, *J. Geophys. Res.*, *109*, D08303, doi:10.1029/2003JD004218.

Alexander, B., J. Savarino, C. C. W. Lee, R. J. Park, D. J. Jacob, Q. Li, R. M. Yantosca, and M. H. Thiemens (2005), Sulfate formation in sea-salt aerosols: Constraints from oxygen isotopes, *J. Geophys. Res.*, *110*, D10307, doi:10.1029/2004JD005659.

Andronache, C., W. L. Chameides, D. D. Davis, B. E. Anderson, R. F. Pueschel, A. R. Bandy, D. C. Thornton, R. W. Talbot, P. Kasibhatla, and C. S. Kiang (1997), Gas-to-particle conversion of tropospheric sulfur as estimated from observations in the western North Pacific during PEM-West B, *J. Geophys. Res.*, *102*(D23), 28,511–28,538.

Baker, A. R., T. D. Jickells, M. Witt, and K. L. Linge (2006), Trends in the solubility of iron, aluminium, manganese and phosphorus in aerosol collected over the Atlantic Ocean, *Mar. Chem.*, *98*(1), 43–58.

Barrie, L. A., et al. (2001), A comparison of large-scale atmospheric sulphate aerosol models (COSAM): Overview and highlights, *Tellus Ser. B*, *53*, 615–645.

Bauer, S. E., and D. Koch (2005), Impact of heterogeneous sulfate formation at mineral dust surfaces on aerosol loads and radiative forcing in the Goddard Institute for Space Studies general circulation model, *J. Geophys. Res.*, *110*(D17), D17202, doi:10.1029/2005JD005870.

Behra, P., and L. Sigg (1990), Evidence for redox cycling of iron in atmospheric water droplets, *Nature*, *344*, 419–421.

Bengtsson, S., and I. Bjerle (1975), Catalytic-oxidation of sulfite in diluted aqueous-solutions, *Chem. Eng. Sci.*, *30*(11), 1429–1435.

Benkovitz, C. M., M. T. Scholtz, J. Pacyna, L. Tarrasón, J. Dignon, E. C. Voldner, P. A. Spiro, J. A. Logan, and T. E. Graedel (1996), Global, gridded inventories for anthropogenic emissions of sulfur and nitrogen, *J. Geophys. Res.*, *101*(D22), 29,239–29,253.

Berglund, J., S. Fronaeus, and L. I. Elding (1993), Kinetics and mechanism for manganese-catalyzed oxidation of sulfur(Iv) by oxygen in aqueous-solution, *Inorg. Chem.*, *32*(21), 4527–4538.

Bond, T. C., D. G. Streets, K. F. Yarber, S. M. Nelson, J.-H. Woo, and Z. Klimont (2004), A technology-based global inventory of black and organic carbon emissions from combustion, *J. Geophys. Res.*, *109*, D14203, doi:10.1029/2003JD003697.

Bonnet, S., and C. Guieu (2004), Dissolution of atmospheric iron in seawater, *Geophys. Res. Lett.*, *31*(3), L03303, doi:10.1029/2003GL018423.

Bopp, L., K. E. Kohfeld, C. L. Quere, and O. Aumont (2003), Dust impact on marine biota and atmospheric $CO_2$ during glacial periods, *Paleoceanography*, *18*(2), 1046, doi:10.1029/2002PA000810.

Brenninkmeijer, C. A. M., C. Janssen, J. Kaiser, T. Röckmann, T. S. Rhee, and S. S. Assonov (2003), Isotope effects in the chemistry of atmospheric trace compounds, *Chem. Rev.*, *102*(12), 5125–5161.

Chatfield, R. B., and P. J. Crutzen (1990), Are there interactions of iodine and sulfur species in marine air photochemistry?, *J. Geophys. Res.*, *95*(D13), 22,319–22,341.

Chen, Y., and R. L. Siefert (2003), Determinations of various types of labile atmospheric iron over remote oceans, *J. Geophys. Res.*, *108*(D24), 4774, doi:10.1029/2003JD003515.

Chen, Y., and R. L. Siefert (2004), Seasonal and spatial distributions and dry deposition fluxes of atmospheric total and labile iron over the tropical and subtropical North Atlantic Ocean, *J. Geophys. Res.*, *109*, D09305, doi:10.1029/2003JD003958.

Chin, M., R. B. Rood, S.-J. Lin, F.-F. Muller, and A. M. Thompson (2000), Atmospheric sulfur cycle simulated in the global model GOCART: Model description and global properties, *J. Geophys. Res.*, *105*(D20), 24,671–24,687.

Chughtai, A. R., M. E. Brooks, and D. M. Smith (1993), Effect of metal-oxides and black carbon (soot) on $SO_2/O_2/H_2O$ reaction systems, *Aerosol Sci. Tech.*, *19*(2), 121–132.

Claquin, T., M. Schulz, and Y. J. Balkanski (1999), Modeling the mineralogy of atmospheric dust sources, *J. Geophys. Res.*, *104*(D18), 22,243–22,256.

Coichev, N., K. B. Reddy, and R. Vaneldik (1992), The synergistic effect of manganese(II) in the sulfite-induced autoxidation of metal-ions and complexes in aqueous-solution, *Atmos. Environ. A Gen. Topics*, *26*(13), 2295–2300.

deMeij, A., M. Krol, F. Dentener, E. Vignati, C. Cuvelier, and P. Thunis (2006), The sensitivity of aerosol in Europe to two different emission inventories and temporal distribution of emissions, *Atmos. Chem. Phys.*, *6*, 4287–4309.

DeMore, W. B., S. P. Sander, D. M. Golden, R. F. Hampson, M. J. Kurylo, C. J. Howard, A. R. Ravishankara, C. E. Kolb, and M. J. Molina (1997), Chemical kinetics and photochemical data for use in stratospheric modeling, *JPL Publ.*, *97-4*, 1–278.

Dentener, F., J. Williams, and S. Metzger (2002), Aqueous phase reaction of $HNO_4$: The impact on tropospheric chemistry, *J. Atmos. Chem.*, *41*, 109–134.

Desboeufs, K. V., A. Sofikitis, R. Losno, J. L. Colin, and P. Ausset (2005), Dissolution and solubility of trace metals from natural and anthropogenic aerosol particulate matter, *Chemosphere*, *58*(2), 195–203.

Deutsch, F., P. Hoffmann, and H. M. Ortner (1997), Analytical characterization of manganese in rainwater and snow samples, *Fresenius J. Anal. Chem.*, *357*(1), 105–111.

Dubey, M. K., R. Mohrschladt, N. M. Donahue, and J. G. Anderson (1997), Isotope-specific kinetics of hydroxyl radical (OH) with water ($H_2O$): Testing models of reactivity and atmospheric fractionation, *J. Phys. Chem. A*, *101*, 1494–1500.

Erel, Y., S. O. Pehkonen, and M. R. Hoffmann (1993), Redox chemistry of iron in fog and stratus clouds, *J. Geophys. Res.*, *98*(D10), 18,423–18,434.

Fairlie, T. D., D. J. Jacob, and R. J. Park (2007), The impact of transpacific transport of mineral dust in the United States, *Atmos. Environ.*, *41*, 1251–1266.

Farquhar, J., J. Savarino, T. L. Jackson, and M. H. Thiemens (2000), Evidence of atmospheric sulphur in the Martian regolith from sulphur isotopes in meteorites, *Nature*, *404*, 50–52.

Feichter, J., E. Kjellstrom, H. Rodhe, F. Dentener, J. Lelieveld, and G. J. Roelofs (1996), Simulation of the tropospheric sulfur cycle in a global climate model, *Atmos. Environ.*, *30*(10–11), 1693–1707.

Feingold, G., G. J. Frost, and A. R. Ravishankara (2002), Role of $NO_3$ in sulfate production in wintertime northern latitudes, *J. Geophys. Res.*, *107*(D22), 4640, doi:10.1029/2002JD002288.

Fogelman, K. D., D. M. Walker, and D. W. Margerum (1989), Non-metal redox kinetics—Hypochlorite and hypochlorous acid reactions with sulfite, *Inorg. Chem.*, *28*, 986–993.

Formenti, P., M. O. Andreae, L. Lange, G. Roberts, J. Cafmeyer, I. Rajta, W. Maenhaut, B. N. Holben, P. Artaxo, and J. Lelieveld (2001), Saharan dust in Brazil and Suriname during the Large-Scale Biosphere-Atmosphere Experiment in Amazonia (LBA) - Cooperative LBA Regional Experiment (CLAIRE) in March 1998, *J. Geophys. Res.*, *106*(D14), 14,919–14,934.

Fung, I. Y., S. K. Meyn, I. Tegen, S. C. Doney, J. G. John, and J. K. B. Bishop (2000), Iron supply and demand in the upper ocean, *Global Biogeochem. Cycles*, *14*(2), 697–700.

Fuzzi, S., et al. (2007), Overview of the inorganic and organic composition of size-segregated aerosol in Rondonia, Brazil, from the biomass-burning period to the onset of the wet season, *J. Geophys. Res.*, *112*, D01201, doi:10.1029/2005JD006741.

Gerber, H. E. (1985), *Relative-humidity Parameterization of the Nave Aerosol Model* (NAM), Natl. Res. Lab., Washington, D. C.

Graedel, T. E., and C. J. Weschler (1981), Chemistry within aqueous atmospheric aerosols and raindrops, *Rev. Geophys.*, *19*(4), 505–539.

Graedel, T. E., M. L. Mandich, and C. J. Weschler (1986), Kinetic model studies of atmospheric droplet chemistry: 2. Homogeneous transition metal chemistry in raindrops, *J. Geophys. Res.*, *91*(D4), 5205–5221.

Grgic, I., V. Hudnik, M. Bizjak, and J. Levec (1991), Aqueous S(IV) oxidation. 1. Catalytic effects of some metal-ions, *Atmos. Environ. A Gen. Topics*, *25*(8), 1591–1597.

Grgic, I., V. Hudnik, M. Bizjak, and J. Levec (1992), Aqueous S(IV) oxidation. 2. Synergistic effects of some metal-ions, *Atmos. Environ. A Gen. Topics*, *26*(4), 571–577.

Guieu, C., R. Duce, and R. Arimoto (1994), Dissolved input of manganese to the ocean—Aerosol source, *J. Geophys. Res.*, *99*(D9), 18,789–18,800.

Guo, Z. G., J. L. Feng, M. Fang, H. Y. Chen, and K. H. Lau (2002), The elemental and organic characteristics of PM2.5 in Asian dust episodes in Qingdao, China, *Atmos. Environ.*, *38*(6), 909–919.

Hand, J. L., N. M. Mahowald, Y. Chen, R. L. Siefert, C. Luo, A. Subramaniam, and I. Fung (2004), Estimates of atmospheric-processed soluble iron from observations and a global mineral aerosol model: Biogeochemical implications, *J. Geophys. Res.*, *109*, D17205, doi:10.1029/2004JD004574.

Hao, Y., Z. Guo, Z. Yang, M. Fang, and J. Feng (2007), Seasonal variation and sources of various elements in the atmospheric aerosols in Qingdao, China, *Atmos. Res.*, *85*, 27–37.

Hoffmann, M. R., and D. J. Jacob (1984), Kinetics and mechanisms of the catalytic oxidation of dissolved sulfur dioxide in aqueous solution: An application to nighttime fog water chemistry, in *$SO_2$, NO, and $NO_2$ Oxidation Mechanisms: Atmospheric Considerations*, edited by J. G. Calvert, pp. 63–100, Elsevier, New York.

Hofmann, H., P. Hoffmann, and K. H. Lieser (1991), Transition metals in atmospheric aqueous samples, analytical determination and speciation, *Fresenius J. Anal. Chem.*, *340*, 591–597.

Holt, B. C., R. Kumar, and P. T. Cunningham (1981), Oxygen-18 study of the aqueous-phase oxidation of sulfur dioxide, *Atmos. Environ.*, *15*(4), 557–566.

Iversen, T., and E. Joranger (1985), Arctic air pollution and large scale atmospheric flows, *Atmos. Environ.*, *19*, 2099–2108.

Jacob, D. J., and M. R. Hoffmann (1983), A dynamic model for the production of $H^+$, $NO_3^-$, and $SO_4^{2-}$ in urban fog, *J. Geophys. Res.*, *88*(C11), 6611–6621.

Jacob, D. J., J. M. Waldman, J. W. Munger, and M. R. Hoffmann (1984), A field investigation of physical and chemical mechanisms affecting pollutant concentrations in fog droplets, *Tellus Ser. B*, *36*(4), 272–285.

Jacob, D. J., E. W. Gottlieb, and M. J. Prather (1989), Chemistry of a polluted cloudy boundary-layer, *J. Geophys. Res.*, *94*(D10), 12,975–13,002.

Janssen, C., J. Guenther, and D. Krankowsky (1999), Relative formation rates of $^{50}O_3$ and $^{52}O_3$ in $^{16}O$-$^{18}O$ mixtures, *J. Chem. Phys.*, *111*(16), 7179–7182.

Johansen, A. M., R. L. Siefert, and M. R. Hoffmann (2000), Chemical composition of aerosols collected over the tropical North Atlantic Ocean, *J. Geophys. Res.*, *105*(D12), 15,277–15,312.

Johnston, J. C., and M. H. Thiemens (1997), The isotopic composition of tropospheric ozone in three environments, *J. Geophys. Res.*, *102*(D21), 25,395–25,404.

Kasibhatla, P., W. L. Chameides, and J. St. John (1997), A three-dimensional global model investigation of seasonal variations in the atmospheric burden of anthropogenic sulfate aerosols, *J. Geophys. Res.*, *102*(D3), 3737–3759.

Kotronarou, A., and L. Sigg (1993), $SO_2$ oxidation in atmospheric water—Role of Fe(II) and effect of ligands, *Environ. Sci. Technol.*, *27*(13), 2725–2735.

Krankowsky, D., F. Bartecki, G. G. Klees, K. Mauersberger, K. Schellenback, and J. Stehr (1995), Measurement of heavy isotope enrichment in tropospheric ozone, *Geophys. Res. Lett.*, *22*(13), 1713–1716.

Kubilay, N., and A. C. Saydam (1995), Trace elements in atmospheric particulates over the eastern Mediterranean: Concentrations, sources and temporal variability, *Atmos. Environ.*, *29*(17), 2289–2300.

Kumala, M., L. Pirjoia, and J. M. Makela (2000), Stable sulphate clusters as a source of new atmospheric particles, *Nature*, *404*, 66–69.

Lee, Y. N., and S. E. Schwartz (1983), Kinetics of oxidation of aqueous sulfur (IV) by nitrogen dioxide, in *Precipitation Scavenging, Dry Deposition and Resuspension, Proceedings of the Fourth International Conference, Santa Monica, California, 29 November– 3 December 1982*, edited by H. Pruppacher, R. Semonin, and a. W. G. N. Slinn, pp. 453–470, Elsevier, New York.

Lee, C. C. W., and M. H. Thiemens (2001), The $\delta^{17}O$ and $\delta^{18}O$ measurements of atmospheric sulfate from a coastal and high alpine region: A mass-independent isotopic anomaly, *J. Geophys. Res.*, *105*(D15), 17,359–17,373.

Lee, C. C. W., J. Savarino, H. Cachier, and M. H. Thiemens (2002), Sulfur ($^{32}S$,$^{33}S$,$^{34}S$,$^{36}S$) and oxygen ($^{16}O$,$^{17}O$,$^{18}O$) isotopic ratios of primary sulfate produced from combustion processes, *Tellus Ser. B*, *54*(3), 193–200.

Liu, H., D. J. Jacob, I. Bey, and R. M. Yantosca (2001), Constraints from $^{210}Pb$ and $^{7}Be$ on wet deposition and transport in a global three-dimensional chemical tracer model driven by assimilated meteorological fields, *J. Geophys. Res.*, *106*(D11), 12,109–12,128.

Liu, C. L., J. Zhang, and Z. B. Shen (2002), Spatial and temporal variability of trace metals in aerosol from the desert region of China and the Yellow Sea, *J. Geophys. Res.*, *107*(D14), 4215, doi:10.1029/2001JD000635.

Luo, C., N. Mahowald, T. Bond, P. Y. Chuang, P. Artaxo, R. Siefert, Y. Chen, and J. Schauer (2008), Combustion iron distribution and deposition, *Global Biogeochem. Cycles*, *22*, GB1012, doi:10.1029/2007GB002964.

Lyons, J. R. (2001), Transfer of mass-independent fractionation in ozone to other oxygen-containing radicals in the atmosphere, *Geophys. Res. Lett.*, *28*, 3231–3234.

Mackie, D. S., P. W. Boyd, K. A. Hunter, and G. H. McTanish (2005), Simulating the cloud processing of iron in Australian dust: pH and dust concentration, *Geophys. Res. Lett.*, *32*, L06809, doi:10.1029/2004GL022122.

Mahowald, N. M., A. R. Baker, G. Bergametti, N. Brooks, R. A. Duce, T. D. Jickells, N. Kubilay, J. M. Prospero, and I. Tegen (2005), Atmospheric global dust cycle and iron inputs to the ocean, *Global Biogeochem. Cycles*, *19*, GB4025, doi:10.1029/2004GB002402.

Martin, L. R. (1984), Kinetic studies of sulfite oxidation in aqueous solution, in *$SO_2$, NO, and $NO_2$ Oxidation Mechanisms: Atmospheric Considerations*, edited by J. G. Calvert, pp. 63–100, Butterworth Publ., Stoneham, Mass.

Martin, L. R., and M. W. Hill (1987a), The iron catalyzed oxidation of sulfur: Reconciliation of the literature rates, *Atmos. Environ.*, *25A*, 1487–1490.

Martin, L. R., and M. W. Hill (1987b), The effect of ionic strength on the manganese catalyzed oxidation of sulfur(IV), *Atmos. Environ.*, *21*, 2267–2270.

Martin, L. R., and T. W. Good (1991), Catalyzed oxidation of sulfur dioxide in solution: The iron-manganese synergism, *Atmos. Environ.*, *25A*, 2395–2399.

Matsuhisa, Y., J. R. Goldsmith, and R. N. Clayton (1978), Mechanisms of hydrothermal crystallization of quartz at 250C and 15kbar, *Geochim. Cosmochim. Acta*, *42*, 173–182.

Mauersberger, K., B. Erbacher, D. Krankowsky, J. Gunther, and R. Nickel (1999), Ozone isotope enrichment: Isotopomer-specific rate coefficients, *Science*, *283*, 370–372.

McCabe, J. R., J. Savarino, B. Alexander, S. Gong, and M. H. Thiemens (2006), Isotopic constraints on non-photochemical sulfate production in the Arctic winter, *Geophys. Res. Lett.*, *33*, L05810, doi:10.1029/2005GL025164.

Nenes, A., S. N. Pandis, and C. Plinis (1998), ISORROPIA: A new thermodynamic equilibrium model for multiphase multicomponent inorganic aerosols, *Aquat. Geochem.*, *4*, 123–152.

Park, R. J., D. J. Jacob, B. D. Field, R. M. Yantosca, and M. Chin (2004), Natural and transboundary pollution influences on sulfate-nitrate-ammonium aerosols in the United States: Implications for policy, *J. Geophys. Res.*, D15204, doi:10.1029/2003JD004473.

Pehkonen, S. O., Y. Erel, and M. R. Hoffmann (1992), Simultaneous spectrophotometric measurement of Fe(II) and Fe(III) in atmospheric water, *Environ. Sci. Technol.*, *26*(9), 1731–1736.

Pickering, W. F. (1996), General strategies for speciation, in *Chemical Speciation in the Environment*, edited by A. M. Ure and C. M. Davidson, pp. 9–32, Blackwell, Malden, Mass.

Podkrajsek, B., I. Grgic, J. Tursic, and G. Bercic (2006), Influence of atmospheric carboxylic acids on catalytic oxidation of sulfur(IV), *J. Atmos. Chem.*, *54*(2), 103–120.

Quinn, P. K., G. Shaw, E. Andrews, E. G. Dutton, T. Ruoho-Airola, and L. Gong (2007), Arctic haze: Current trends and knowledge gaps, *Tellus Ser. B*, *59*(1), 99–114.

Rao, X., and J. L. Collett (1998), The drop size-dependence of iron and manganese concentrations in clouds and fogs: Implications for sulfate production, *J. Atmos. Chem.*, *30*(2), 273–289.

Rasch, P. J., et al. (2000), A comparison of scavenging and deposition processes in global models: Results from the WCRP Cambridge Workshop of 1995, *Tellus Ser. B*, *52*(4), 1025–1056.

Roelofs, G. J., et al. (2001), Analysis of regional budgets of sulfur species modeled for the COSAM exercise, *Tellus Ser. B*, *53*(5), 673–694.

Rotstayn, L. D., and U. Lohmann (2002), Simulation of the tropospheric sulfur cycle in a global model with a physically based cloud scheme, *J. Geophys. Res.*, *107*(D21), 4592, doi:10.1029/2002JD002128.

Salomons, W., and U. Forstner (1984), *Metals in the Hydrocycle*, Springer, New York.

Savarino, J., and M. H. Thiemens (1999), Analytical procedure to determine both $\delta^{18}O$ and $\delta^{17}O$ of $H_2O_2$ in natural water and first measurements, *Atmos. Environ.*, *33*, 3683–3690.

Savarino, J., C. C. W. Lee, and M. H. Thiemens (2000), Laboratory oxygen isotopic study of sulfur (IV) oxidation: Origin of the mass-independent oxygen isotopic anomaly in atmospheric sulfates and sulfate mineral deposits on Earth, *J. Geophys. Res.*, *105*(D23), 29,079–29,088.

Savarino, J., S. Bekki, J. Cole-Dai, and M. H. Thiemens (2003), Evidence from sulfate mass independent oxygen isotopic compositions of dramatic changes in atmospheric oxidation following massive volcanic eruptions, *J. Geophys. Res.*, *108*(D21), 4671, doi:10.1029/2003JD003737.

Schwartz, S. E. (1987), Aqueous-Phase Reactions in Clouds, in *The Chemistry of Acid Rain: Sources and Atmospheric Processes*, edited by R. W. Johnson and G. E. Gordon, Am. Chem. Soc., Washington, D. C.

Sedwick, P. N., E. R. Sholkovitz, and T. M. Church (2007), Impact of anthropogenic combustion emissions on the fractional solubility of aerosol iron: Evidence from the Sargasso Sea, *Geochem. Geophys. Geosyst.*, *8*, Q10Q06, doi:10.1029/2007GC001586.

Siefert, R. L., A. M. Johansen, M. R. Hoffmann, and S. O. Pehkonen (1998), Measurements of trace metal (Fe, Cu, Mn, Cr) oxidation states in fog and stratus clouds, *J. Air Waste Manage.*, *48*(2), 128–143.

Sirois, A., and L. A. Barrie (1999), Arctic lower tropospheric aerosol trends and composition at Alert, Canada: 1980–1995, *J. Geophys. Res.*, *104*(D9), 11,599–11,618.

Solomon, S., et al. (2007), Technical summary, in *Climate Change 2007: The Physical Science Basis. Contribution of Working Group I to the Fourth Assessment Report of the Intergovernmental Panel on Climate Change*, edited by S. Solomon et al., Cambridge Univ. Press, New York.

Somerville, R. C. J., and L. A. Remer (1984), Cloud optical thickness feedbacks in the $CO_2$ climate problem, *J. Geophys. Res.*, *89*(D6), 9668–9672.

Spokes, L. J., T. D. Jickells, and B. Lim (1994), Solubilization of aerosol trace metals by cloud processing: A laboratory study, *Geochim. Cosmochim. Acta*, *58*(15), 3281–3287.

Stockwell, W. R., and J. G. Calvert (1983), The mechanism of the HO-$SO_2$ reaction, *Atmos. Environ.*, *17*(11), 2231–2235.

Sundqvist, H., E. Berge, and J. E. Kristiansson (1989), Condensation and cloud parameterization studies with a mesoscale numerical weather prediction model, *Mon. Weather Rev.*, *117*, 1641–1657.

Taylor, S. R., and S. M. McLennan (1985), *The Continental Crust: Its Composition and Evolution*, 312 pp., Blackwell, Malden, Mass.

Thiemens, M. H. (1999), Mass-independent isotope effects in planetary atmospheres and the early solar system, *Science*, *283*, 341–345.

Tursic, J., I. Grgic, and B. Podkrajsek (2003), Influence of ionic strength on aqueous oxidation of $SO_2$ catalyzed by manganese, *Atmos. Environ.*, *37*(19), 2589–2595.

Usher, C. R., A. E. Michel, and V. H. Grassian (2003), Reactions on mineral dust, *Chem. Rev.*, *103*(12), 4883–4939.

Vogt, R., P. J. Crutzen, and R. Sander (1996), A mechanism for halogen release from sea-salt aerosol in the marine boundary layer, *Nature*, *383*, 327–330.

von Glasow, R., R. Sander, A. Bott, and P. J. Crutzen (2002), Modeling halogen chemistry in the marine boundary layer: 2. Interactions with sulfur and the cloud-covered MBL, *J. Geophys. Res.*, *107*(D17), 4323, doi:10.1029/2001JD000943.

Wang, Y. H., D. J. Jacob, and J. A. Logan (1998), Global simulation of tropospheric $O_3$-NOx hydrocarbon chemistry: 1. Model formulation, *J. Geophys. Res.*, *103*(D9), 10,713–10,725.

Warneck, P. (1999), The relative importance of various pathways for the oxidation of sulfur dioxide and nitrogen dioxide in sunlit continental fair weather clouds, *Phys. Chem. Chem. Phys.*, *1*, 5471–5483.

Weber, R. J., G. Chen, D. D. Davis, R. L. Mauldin III, D. J. Tanner, F. L. Eisele, A. D. Clarke, D. C. Thornton, and A. R. Bandy (2001), Measurements of enhanced $H_2SO_4$ and 3–4 nm particles near a frontal cloud during the First Aerosol Characterization Experiment (ACE 1), *J. Geophys. Res.*, *106*(D20), 24,107–124,117.

Weschler, C. J., M. L. Mandich, and T. E. Graedel (1986), Speciation, photosensitivity, and reactions of transition metal ions in atmospheric droplets, *J. Geophys. Res.*, *91*(D4), 5189–5204.

Weseley, M. L. (1989), Parameterization of surface resistances to gaseous dry deposition in regional-scale numerical-models, *Atmos. Environ.*, *23*, 1293–1304.

Wu, J., and E. Boyle (2002), Iron in the Sargasso Sea: Implications for the processes controlling dissolved Fe distribution in the ocean, *Global Biogeochem. Cycles*, *16*(4), 1086, doi:10.1029/2001GB001453.

Yermakov, A. N., G. A. Poskrebyshev, and A. P. Purmal (1997), On the kinetics of bisulfite autoxidation catalyzed by manganese(II) ions, *Prog. React. Kinet.*, *22*(2), 141–171.

Zhang, L., S. Gong, J. Padro, and L. Barrie (2001), A size-segregated particle dry deposition scheme for an atmospheric aerosol module, *Atmos. Environ.*, *35*, 549–560.

Zhu, X. R., J. M. Prospero, and F. J. Millero (1997), Diel variability of soluble Fe(II) and soluble total Fe in North African dust in the trade winds at Barbados, *J. Geophys. Res.*, *102*(D17), 21,297–21,305.

Zhu, L., A. Nenes, P. H. Wine, and J. M. Nicovich (2006), Effects of aqueous organosulfur chemistry on particulate methanesulfonate to non–sea salt sulfate ratios in the marine atmosphere, *J. Geophys. Res.*, *111*, D05316, doi:10.1029/2005JD006326.

Zhuang, G., Z. Yi, R. A. Duce, and P. R. Brown (1992a), Chemistry of iron in marine aerosols, *Global Biogeochem. Cycles*, *6*(2), 161–173.

Zhuang, G., Z. Yi, R. A. Duce, and P. R. Brown (1992b), Link between iron and sulphur cycles suggested by detection of Fe(II) in remote marine aerosols, *Nature*, *355*, 537–539.

Zhuang, G., Z. Yi, and G. T. Wallace (1995), Iron (II) in rainwater, snow, and surface seawater from a coastal environment, *Mar. Chem.*, *50*, 41–50.

Zuo, Y. G., and J. Zhan (2005), Effects of oxalate on Fe-catalyzed photoxidation of dissolved sulfur dioxide in atmospheric water, *Atmos. Environ.*, *39*(1), 27–37.

B. Alexander, Department of Atmospheric Sciences, University of Washington, 408 ATG Building, Seattle, WA 98195-1640, USA. (beckya@u.washington.edu)

S. Gong, Air Quality Research Division, Environment Canada, 4905 Dufferin Street, Downsview, Toronto, ON M3H 5T, Canada.

D. J. Jacob, School of Engineering and Applied Sciences and Department of Earth and Planetary Sciences, Harvard University, Pierce Hall, 29 Oxford Street, Cambridge, MA 02138, USA.

R. J. Park, School of Earth and Environmental Sciences, Seoul National University, 599 Gwanangno, Building 501-506, Gwanak-gu, Seoul 151-742, Korea.